Soft Matter

PAPER

View Article Online
View Journal | View Issue

Open Access Article. Published on 13 December 2021. Downloaded on 1/21/2026 4:01:33 AM.
This article is licensed under a Creative Commons Attribution 3.0 Unported Licence.

Check for updates

Cite this: *Soft Matter*, 2022, **18**, 390

Rheo-SAXS study of shear-induced orientation and relaxation of cellulose nanocrystal and montmorillonite nanoplatelet dispersions†

Pierre Munier,[a] Seyed Ehsan Hadi,[ab] Mo Segad[a] and Lennart Bergström *[a]

Received 3rd June 2021,
Accepted 26th November 2021

DOI: 10.1039/d1sm00837d

rsc.li/soft-matter-journal

The development of robust production processes is essential for the introduction of advanced materials based on renewable and Earth-abundant resources. Cellulose nanomaterials have been combined with other highly available nanoparticles, in particular clays, to generate multifunctional films and foams. Here, the structure of dispersions of rod-like cellulose nanocrystals (CNC) and montmorillonite nanoplatelets (MNT) was probed using small-angle X-ray scattering within a rheological cell (Rheo-SAXS). Shear induced a high degree of particle orientation in both the CNC-only and CNC:MNT composite dispersions. Relaxation of the shear-induced orientation in the CNC-only dispersion decayed exponentially and reached a steady-state within 20 seconds, while the relaxation of the CNC:MNT composite dispersion was found to be strongly retarded and partially inhibited. Viscoelastic measurements and Guinier analysis of dispersions at the shear rate of 0.1 s^{-1} showed that the addition of MNT promotes gel formation of the CNC:MNT composite dispersions. A better understanding of shear-dependent assembly and orientation of multi-component nanoparticle dispersions can be used to process materials with improved mechanical and functional properties.

Introduction

Nanomaterials based on renewable and abundant resources are attracting a large and rapidly growing research interest.[1,2] Cellulose nanomaterials (CNMs) are elongated cellulose nanoparticles[3] that display an attractive combination of properties, *e.g.* high stiffness and mechanical strength, low density, anisotropic thermal conductivity, and chemical versatility,[4,5] and are found in a variety of natural sources from which extraction routes are continuously being developed.[6,7] Cellulose nanocrystals (CNC) are particularly interesting due to their ability to self-assemble into chiral nematic phases[8,9] with useful optical properties,[10,11] and as a reinforcing additive in various composites.[12]

Intrinsic shortcomings of CNMs, such as their poor moisture resistance,[13,14] can be mitigated by combining CNMs with other widely abundant nanomaterials *e.g.* different clays like montmorillonite (MNT), vermiculite, kaolinite, and saponite.[15] Indeed, organic–inorganic hybrid and composite materials with superior properties to the constituent compounds are often found in nature and have been developed and utilized by man throughout history.[16] CNMs combined with clays such as montmorillonite have resulted in composites with low vapor permeability[17,18] and high flame retardancy.[19]

Processing of CNC-based dispersions into functional nanocomposites can be performed using different techniques, *e.g.* hydrodynamic alignment,[20] fiber spinning,[21–23] roll to roll coating,[24] ice-templating,[25] and 3D printing.[26–30] Optimization of shear-based processing methods requires that the rheological behavior and how shear influences and controls the structure of the processed systems are well understood. Shear-induced orientation and relaxation can be probed by coupling rheological measurements with a light, neutron, or small-angle X-ray scattering (SAXS), *i.e.* Rheo-SAXS. The shear-induced orientation of CNC-only and MNT-only dispersions have been studied previously[31–36] but the orientation and relaxation of mixtures of CNC with other nanoparticles have not been reported.

In this study, we have probed the orientation and relaxation of CNC and montmorillonite nanoplatelets (MNT) dispersions by Rheo-SAXS. We show that shear induced a high degree of orientation in the CNC-only, MNT-only, and CNC:MNT composite dispersions. The CNC-only dispersion displayed an exponential time-dependency of the relaxation of the shear-induced orientation, whereas the relaxation of the CNC:MNT composite dispersions was found to be strongly retarded. Viscoelastic

[a] *Department of Materials and Environmental Chemistry, Stockholm University, Stockholm, 10691, Sweden. E-mail: lennart.bergstrom@mmk.su.se*
[b] *Wallenberg Wood Science Center, Department of Materials and Environmental Chemistry, Stockholm University, Stockholm, 10691, Sweden*

† Electronic supplementary information (ESI) available. See DOI: 10.1039/d1sm00837d

This journal is © The Royal Society of Chemistry 2022

Open Access Article. Published on 13 December 2021. Downloaded on 1/21/2026 4:01:33 AM.
This article is licensed under a Creative Commons Attribution 3.0 Unported Licence.

measurements and Guinier analysis provided support that the CNC:MNT composite dispersion forms a gel.

Materials and methods

The CNC and MNT (under the name Cloisite Na+™) were obtained as powders from CelluForce Inc. and BYK Additives, respectively, and used without further purification. CNC and MNT were dispersed in deionized water under mechanical stirring to yield dispersions with concentrations around 4 wt% for CNC and 1.6 wt% for MNT. The MNT dispersion was subjected to high-shear mixing using Ultra Turrax™ and dialyzed against ultrapure water for 7 days, using cellulosic tubular membranes (Sigma-Aldrich) with a molecular weight cut-off of 14 000 Da, after which the sediment was discarded. When needed, the concentrations of the aqueous dispersions were adjusted by removing water by evaporation. CNC:MNT composite dispersions were obtained by mixing the desired amounts of the CNC and MNT dispersions using magnetic stirring complemented with vortex mixing and/or Ultra Turrax™ mixing.

The length and thickness of the CNC particles were determined by tapping-mode Atomic Force Microscopy micrographs (AFM, Dimension 3100, Bruker, USA), of 100 particles deposited onto freshly cleaved mica disks from dilute dispersions (Fig. S1, ESI†). The diameter of the MNT platelets deposited onto carbon-coated copper was estimated from Transmission Electron Microscopy images (TEM, JEM-2100F, 200 kV) of 70 particles (Fig. S2, ESI†). The X-ray diffraction (XRD) pattern of MNT was collected using an X-ray diffractometer (Panalytical X'PERT PRO). The surface charge density of the sulfonated CNCs was estimated by conductometric titration of the sulfate half-ester groups. After sonication and dialysis, the surface groups were first protonated using a strongly acidic ion-exchange resin (Dowex Marathon C™, H+ form, Alfa Aesar),[37–39] after which titration was conducted in a 100 mM sodium chloride solution, using sodium hydroxide as the titrant. The zeta potentials of CNC and MNT dispersed in water were measured using a Zetasizer Nano ZS (Malvern Instruments Ltd). Small-Angle X-ray Scattering (SAXS) experiments combined with rheology (Rheo-SAXS) were conducted at the SWING beamline at Synchrotron Soleil, France (Proposal 20171034).

The dispersions were subjected to a succession of constant shearing and low-shear relaxation regimes, using a programmed measurement. After loading, the samples were allowed to rest inside the chamber for one minute at a shear rate of 0.1 s^{-1}. After the initial resting, the dispersions were subjected to cycles consisting of one minute of shearing and five minutes of relaxation. The imposed shear rate was increased by one order of magnitude at each successive shearing regime, while the shear rate was fixed at 0.1 s^{-1} during the low-shear, relaxation regime (Fig. 1c).

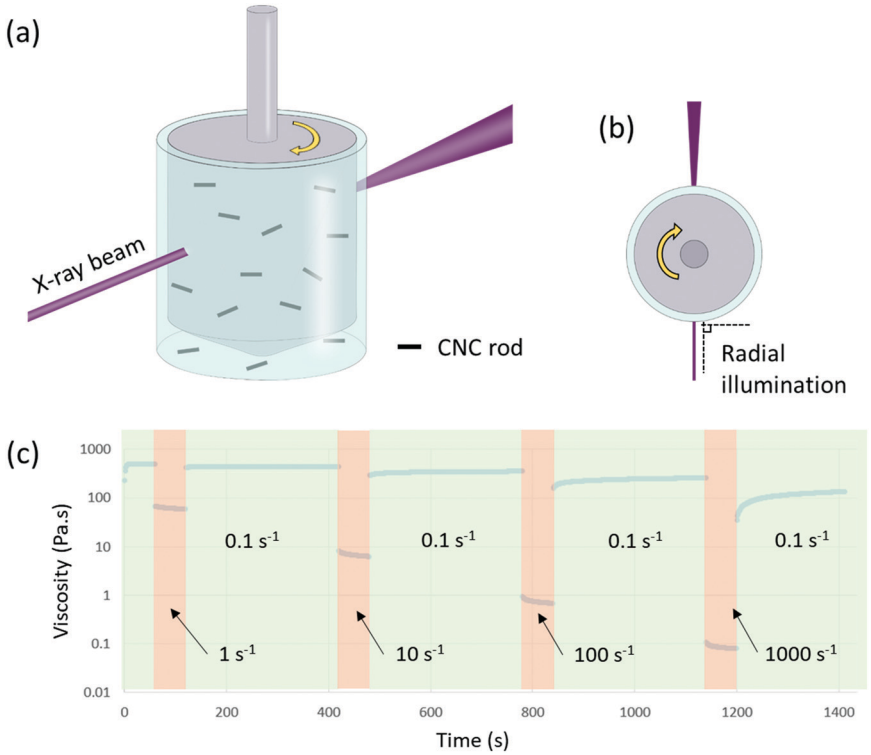

Fig. 1 Rheo-SAXS experiments. (a) Schematic illustration of the concentric cylinder rheological cell used for the Rheo-SAXS experiments. (b) Top-view schematic highlighting the radial illumination of the dispersions, perpendicular to the flow direction and parallel to the velocity gradient. (c) Representative viscosity (in logarithmic scale) *versus* time graph from a Rheo-SAXS experiment for a composite dispersion containing 3.6 wt% CNC and 2.5 wt% MNT. The green zones represent low-shear relaxation regimes (0.1 s^{-1}) and the red zones represent regimes in which the dispersions have been subjected to the shear rates shown in the figure.

Open Access Article. Published on 13 December 2021. Downloaded on 1/21/2026 4:01:33 AM.
This article is licensed under a Creative Commons Attribution 3.0 Unported Licence.

The rheometer used at the beamline was an MCR 501 (Anton Paar) equipped with a polycarbonate concentric cylinder bob and cup geometry with a 10 mm diameter and a 0.5 mm gap. The geometry was radially illuminated by a 388 × 8.1 μm^2 X-ray beam at an energy of 12 keV. The SAXS data were recorded by an EigerX4M detector in a vacuum with a 75 × 75 μm^2 pixel size, placed 3.5 m away from the sample, and covering wave vectors (q) ranging from 0.00154 to 0.31702 $Å^{-1}$. Each frame corresponded to 250 ms of exposure time and 750 ms of resting time, allowing for the collection of one frame per second. The data were reduced and azimuthally integrated using the Foxtrot 3.5.10 software provided at the beamline. All SAXS data processing, including background subtraction and fittings, was done with RAW 2.1.1,[40] ATSAS 3.0.4,[41] SasView 5.0.4, and OriginLab. Steady-shear and oscillatory measurements were performed using a Physica MCR 301 rheometer (Anton Paar), at a temperature of 25 °C. The selected geometry was a smooth metallic concentric cylinder bob and cup geometry (CC27/T200/SS) with a 27 mm diameter and a 1.13 mm gap. The steady shear measurements were performed between 0.001 and 1000 s^{-1}. The critical strain of CNC-only 3.6 wt% dispersion at 1 rad s^{-1} is estimated to be 5.9% (see Fig. S3, ESI†), and the oscillatory measurements were all performed in the linear viscoelastic region at a strain of 3% and a temperature of 25 °C.

Results and discussion

Characterization of dispersions and Rheo-SAXS experiments

The shear-induced orientation of cellulose nanocrystals (CNC) and montmorillonite platelets (MNT) was investigated by so-called Rheo-SAXS experiments, where small-angle X-ray scattering (SAXS) patterns were collected of aqueous dispersions during and after shearing in an X-ray-transparent concentric cylindrical cell (Fig. 1a). The SAXS patterns were obtained perpendicular to the rotational flow, allowing particle orientation in the flow direction to be assessed (Fig. 1b).

The CNC particles are stiff and rod-shaped, with an average length of 173 ± 41 nm, and a rectangular cross-section, of which the shorter edge has an average thickness of 4.3 ± 0.8 nm (Fig. S1, ESI†). The corresponding average aspect ratio is 40. The surface of CNC consists of negatively charged sulfate half-ester groups, with a density of 314 μmol g^{-1}, determined by conductometric titration. The zeta potential of the CNC dispersions at pH 6 ranged between −40 and −60 mV, which suggests that the CNC is electrostatically stabilized.[42] The 3.6 wt% CNC dispersions used in this study were birefringent, which is consistent with previous studies of aqueous dispersions of CNC from the same provider, where a fully anisotropic phase was found at concentrations above 3.5 wt%.[39] Anisotropic CNC dispersions have previously been treated as colloidal glass,[43] and the critical concentration for colloidal glass formation,[44,45] for the CNC studied here was estimated to be 2.8 wt%.

The MNT platelets featured a well-defined thickness of about 1 nm,[46] and an average diameter of 122 ± 65 nm of the irregularly shaped disk-like particles. The zeta potential of MNT dispersions at pH 9 was −35 ± 1 mV. All the CNC:MNT composite dispersions displayed negligible sedimentation over a period of several days.

Shear-induced orientation and relaxation

The SAXS patterns of the sheared CNC-containing dispersions revealed structural peaks at q = 0.01–0.03 $Å^{-1}$ after radial integration and subtraction of the background, (Fig. 2a). The shear rate has an insignificant effect on the main peak position of CNC-only dispersion, but the main peak position of the CNC:MNT composite dispersion changed depending on the shear rate (Fig. S4, ESI†). It should be noted that the main peak position and intensity of the CNC:MNT composite dispersion recovered during the relaxation period (Fig. S4, ESI†).

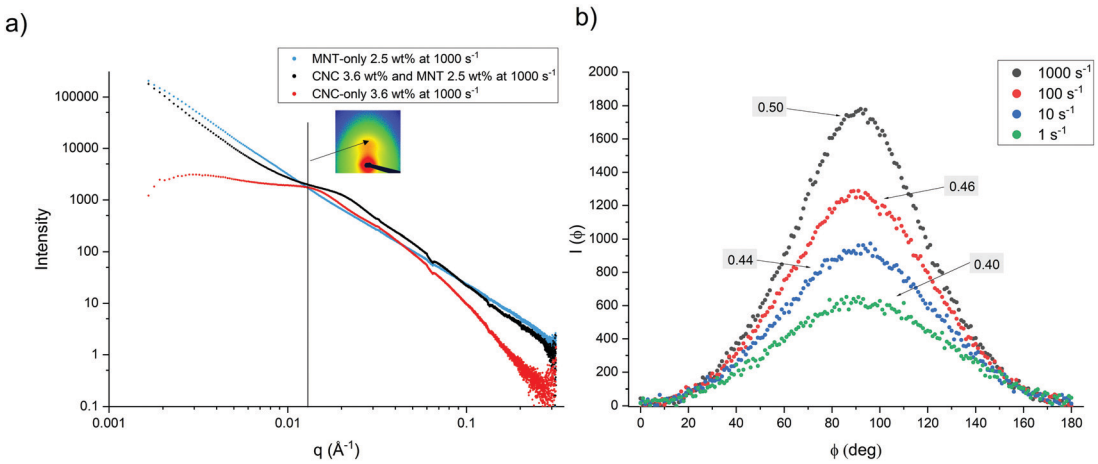

Fig. 2 SAXS patterns and shear-induced particle orientation. (a) Radial integration of 2D SAXS patterns obtained at second 59 of a 60 second shearing of CNC-only, CNC:MNT composite, and MNT-only dispersions at a shear rate of 1000 s^{-1}. Inset: 2D SAXS pattern for the sheared CNC dispersion at a q of 0.0132 $Å^{-1}$. (b) Azimuthal integration of 2D SAXS patterns of CNC-only 3.6 wt% dispersion, subjected to different shear rates (see legend). The corresponding Herman's orientation parameter values are displayed as insets.

 This journal is © The Royal Society of Chemistry 2022

Open Access Article. Published on 13 December 2021. Downloaded on 1/21/2026 4:01:33 AM.
This article is licensed under a Creative Commons Attribution 3.0 Unported Licence.

The 2D SAXS patterns (Fig. 2a, inset) at the center of the structural peak were anisotropic and displayed two brighter spots, which shows that the CNC particles were oriented in the flow direction during shearing. The degree of shear-induced orientation of the CNC and MNT particles were quantified using the annular averages that were obtained by azimuthal integration of the 2D SAXS patterns (Fig. 2b). The Herman's orientation parameter, $\bar{P}_2$, was calculated by curve fitting using eqn (2) and (3) after normalizing $I(\phi)$ with eqn (1):[34,47,48]

$$\int_0^{\frac{\pi}{2}} I(\phi)\sin(\phi)\mathrm{d}(\phi) = 1 \quad (1)$$

$$I(\phi) \cong \sum_{n=0}^{5} a_n P_{2n}(\cos\phi) \quad (2)$$

$$\bar{P}_2 = \frac{a_1}{5} \quad (3)$$

where ϕ and $I(\phi)$ are the azimuthal angle (the integration variable) and its corresponding intensity, which was fitted to a Legendre series expansion, with P_{2n} being even Legendre polynomials and a_n their corresponding coefficients (the fitting parameters). After normalizing the intensities, a_0 = 1, the orientation parameter, $\bar{P}_2$, was obtained from the a_1 coefficient. The $\bar{P}_2$ values can range from −0.5 to 1. When $\bar{P}_2$ = 1, the particles are perfectly vertically oriented, and for randomly oriented particles $\bar{P}_2$ = 0. For horizontally oriented particles $\bar{P}_2$ = −0.5. In this study, the orientation degree of the particles was calculated by shifting the ϕ by −90 degrees, which results in a $\bar{P}_2$ range between 0 and 1, where 0 corresponds to random orientation and a value of 1 corresponds to a perfect orientation of all the particles in the flow direction. Fig. 2b shows that the 3.6 wt% CNC-only dispersion exhibited shear-induced orientation of the rod-like CNC particles at all four investigated shear rates. The $\bar{P}_2$ values increased with increasing shear rate, which shows that the shear-induced orientation in the flow direction increases with increasing shear rate (Fig. 2b).[32] The obtained $\bar{P}_2$ values compared well with those obtained by Haywood *et al.*[34] for a CNC dispersion at a concentration of 5.83 vol% (around 9 wt%). The similar degrees of orientation of these two CNC dispersions despite the significant difference in concentration can be related to the differences in the onset of nematic ordering, with the CNC used by Haywood *et al.* displaying biphasic dispersions from 5.0 wt% and fully anisotropic dispersions only from 10.0 wt%, whereas the CNC we used in this study was already highly anisotropic at 3.6 wt%. The differences in the concentration at which a highly anisotropic phase is obtained can be attributed to the differences in the aspect ratio of CNCs, with an average aspect ratio of 26 for the CNC used by Haywood *et al.*,[34] while the average aspect ratio of the CNC used in this study was 40.

The time-dependent loss of shear-induced orientation was evaluated during the low-shear relaxation regime that followed after the dispersion had been subjected to a 1000 s^{-1} shear rate (see Fig. 1c). Fig. 3a shows azimuthal scattering peaks that were obtained at different times during the low-shear relaxation period for the CNC-only dispersion, while Fig. 3b displays the temporal loss of the orientation of the particles during relaxation for the CNC-only, MNT-only, and CNC:MNT composite dispersions.

The CNC:MNT composite dispersion with a CNC content that was identical to the CNC-only dispersions (3.6 wt%), and an MNT content of 2.5 wt% displayed an initial relatively fast but small decrease of the $\bar{P}_2$ followed by a period of a near-constant $\bar{P}_2$ value (Fig. 3b). The initial fast decay of the alignment may be related to particles of shorter length.[49] The slow decay remained almost constant throughout the studied relaxation period (300 s).

In contrast, the $\bar{P}_2$ value for the CNC-only dispersion displayed a relatively fast exponential decay down to a steady-state

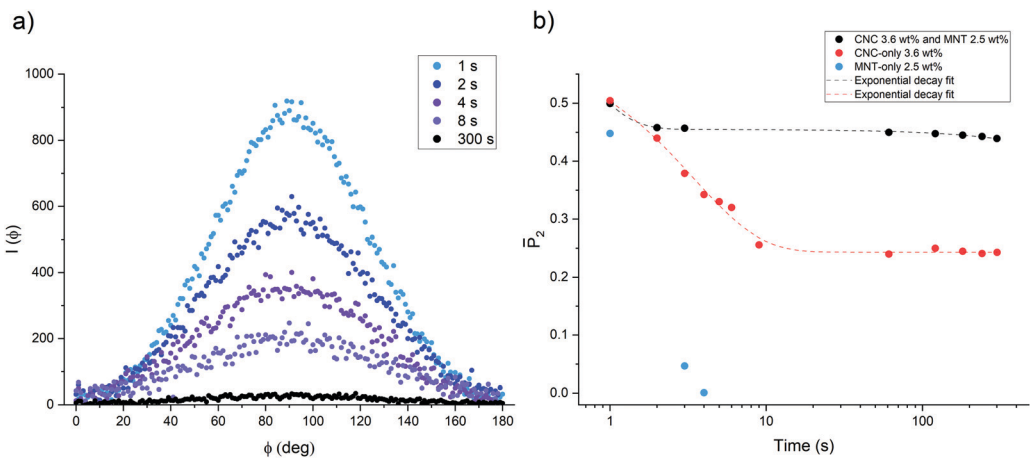

Fig. 3 Relaxation of shear-induced particle orientation. (a) Azimuthal integration of the 2D SAXS patterns of CNC-only 3.6 wt% dispersion at 0.0131 $Å^{-1} < q < 0.0133$ $Å^{-1}$ at different times during the low-shear relaxation period after shearing at 1000 s^{-1}. (b) Herman's orientation parameter of CNC as a function of time for CNC-only, MNT-only and CNC:MNT composite dispersions. The dashed curves represent least squares fit to exponential decay functions. The time at which the shearing was stopped was set to t = 1 s and relates to the state of the dispersion at the very beginning of the relaxation period.

Open Access Article. Published on 13 December 2021. Downloaded on 1/21/2026 4:01:33 AM.
This article is licensed under a Creative Commons Attribution 3.0 Unported Licence.

orientation parameter of around 0.24 after approximately 20 seconds. $\bar{P}_2$ values of the 2.5 wt% MNT-only dispersion showed a very rapid decay, where $\bar{P}_2$ decreased from 0.44 to almost zero after three seconds. Hence, both the CNC-only and MNT-only dispersions relax rapidly after shear-induced alignment.

The rotational diffusion coefficient, D_r, of rod-shaped particles can be estimated by measuring the decay in the Herman's orientation parameter values with respect to time as described by eqn (4):[20,50,51]

$$\bar{P}_2(t) = (\bar{P}_{2,0} - \bar{P}_{2,ss})\exp(-6D_r \cdot t) + \bar{P}_{2,ss} \quad (4)$$

where the $\bar{P}_{2,0}$ is the Herman's orientation parameter just before shearing is stopped and the $\bar{P}_{2,ss}$ is the steady-state Herman's orientation parameter of the dispersion at the shear rate of 0.1 s^{-1}. Using eqn (4), the D_r value of the 3.6 wt% CNC-only dispersion was estimated to be 0.048 ± 0.004 $rad^2\ s^{-1}$. This low extracted D_r value corresponds to previous estimates at high CNC concentrations by Van Rie *et al.* showed that D_r for CNC determined by light scattering decreased from 310 to 0 $rad^2\ s^{-1}$ as the particle concentration increased from 1 to 5 wt%.[52]

The relaxation of the particle orientation in the CNC:MNT composite dispersions is strongly retarded and partially quenched. Using eqn (4), the rotational diffusion coefficient value for the slow relaxation ($D_{r,slow}$) of the CNC 3.6 wt% and 2.5 wt% MNT composite dispersion is estimated to be around $(8.0 \pm 0.6) \times 10^{-5}\ rad^2\ s^{-1}$.

It should be noted that the orientation after high shear of a CNC:MNT composite dispersion with a lower CNC content of 2.5 wt% CNC, and 0.5 wt% MNT (Fig. S5, ESI†), was as high as for the CNC-only 3.6 wt% dispersions. The orientation decreased exponentially with time, with a relaxation time (~5.5 s) which is higher than the relaxation time for the CNC-only 3.6 wt% dispersion (~3.4 s).

Rheological properties of CNC-only, MNT-only, and CNC:MNT composite dispersions

The CNC-only and CNC:MNT composite dispersions displayed a pronounced shear-thinning behavior with a decrease of the viscosity with increasing shear rates of two to three orders of magnitude (Fig. 4a). The shear-thinning behavior confirms that the anisotropic particles orient in the shear direction.[53] The addition of MNT to CNC dispersion increased the viscosity of the dispersion, which suggests that the electrostatic interactions between negatively charged CNC particles and positively charged MNT platelet edges result in aggregation and gel formation.[54] The low-shear viscosity (0.1 s^{-1}) of the composite dispersion containing 3.6 wt% CNC and 2.5 wt% MNT was more than 10 times higher than for the CNC-only dispersion and more than 10 000 times higher than for the MNT-only 2.5 wt% dispersion (Fig. S6, ESI†). Fig. 4b shows The viscoelastic properties of the CNC-only and CNC:MNT composite dispersions were probed by frequency sweep measurements, indicating that the CNC-only dispersion displays a predominantly liquid-like behavior as the storage modulus (G') is lower than the loss modulus (G'') at frequencies below 1 rad s^{-1}. The CNC:MNT composite dispersion, however, displayed a solid-like behavior with the G' being larger than G'' throughout the entire measured frequency range. The pronounced elasticity in the CNC 3.6 wt% and MNT 2.5 wt% composite dispersion compared to the CNC-only dispersion suggests that MNT promotes gel formation. The Guinier plots of the MNT and CNC:MNT composite dispersions at the shear rate of 0.1 s^{-1} (Fig. 5) display an increase in intensity at small values of q, which corroborates that the addition of MNT induces aggregation. In contrast, the CNC-only dispersions display a decrease in intensity, which is characteristic for particle dispersions having strong inter-particle repulsion.[55,56]

Conclusions

The Rheo-SAXS measurements showed that shear induced a high degree of particle orientation in both the CNC-only dispersion containing 3.6 wt% CNC, and the CNC:MNT composite dispersion containing 3.6 wt% CNC and 2.5 wt% MNT. The CNC-only and CNC:MNT composite dispersions displayed a

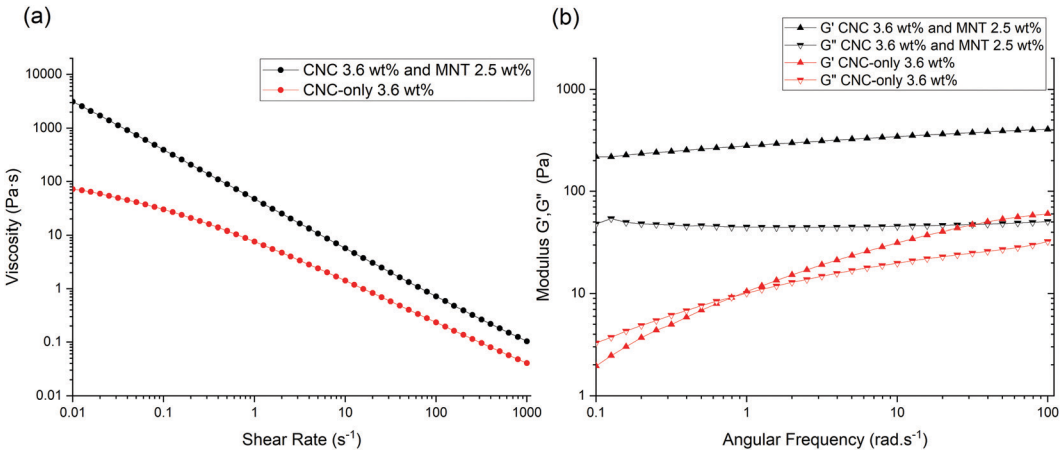

Fig. 4 Rheological properties of the CNC-only and CNC:MNT composite dispersions (a) steady-state shear viscosity against shear rate obtained *via* rotational measurements on CNC-only and CNC:MNT composite dispersions at 25 °C. (b) Storage, G', and loss, G'' moduli *versus* angular frequency for CNC-only and CNC:MNT composite dispersions at 3% strain and 25 °C.

 This journal is © The Royal Society of Chemistry 2022

Open Access Article. Published on 13 December 2021. Downloaded on 1/21/2026 4:01:33 AM.
This article is licensed under a Creative Commons Attribution 3.0 Unported Licence.

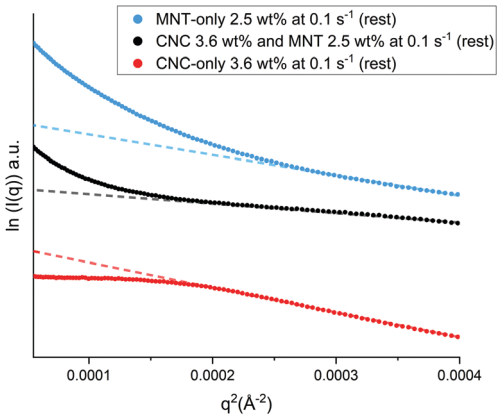

Fig. 5 Guinier plots. Guinier plots of CNC-only, CNC:MNT composite and MNT-only dispersions at 0.1 s^{-1} (rest).

pronounced shear-thinning behavior, which corroborates the shear-induced orientation of the anisotropic particles in the shear direction. The relaxation at low-shear of the shear-induced orientation in the CNC-only dispersion was found to be fast and followed an exponential time-dependency. A rotational diffusion coefficient with a value of 0.048 ± 0.004 rad^2 s^{-1} was extracted from the time-dependent relaxation data for the CNC-only dispersion. Guinier analysis of SAXS data of the dispersions at the shear rate of 0.1 s^{-1} showed that the CNC-only dispersion is dominated by repulsive particle interactions, while the increase in scattered intensity at small values of q for the CNC:MNT composite dispersion suggests that the addition of MNT induces aggregation. The relaxation of the CNC:MNT composite dispersion containing 3.6 wt% CNC and 2.5 wt% MNT was strongly retarded and partially inhibited, and the estimated rotational diffusion coefficient was more than 500 times smaller compared to the CNC-only dispersion. Viscoelastic measurements showed that the CNC-only dispersion displayed a predominantly liquid-like behavior while the CNC:MNT composite dispersion displayed a solid-like behavior, which suggests that the electrostatic interactions between negatively charged CNC particles and positively charged MNT platelet edges result in aggregation and gel formation.

Author contributions

P. M. designed the SAXS experiments, prepared samples, conducted the experiments and the data analysis, and participated in the manuscript writing. S. E. H. prepared samples for the rheology measurements, conducted the experiments and the data analysis, and participated in the manuscript writing. M. S. participated in designing and conducting the synchrotron experiments. L. B. designed the study and participated in the data interpretation and manuscript writing. All authors revised the manuscript.

Conflicts of interest

There are no conflicts to declare.

Acknowledgements

The Swedish Energy Agency (Energimyndigheten, Grant No. 48566-1) and the Wallenberg Wood Science Centre (WWSC) are thanked for providing funding. The SWING beamline staff is thanked for allowing us to collect data at their workstation, and Dr Thomas Bizien is particularly thanked for his support and assistance during and after the beamtime. Luis Valencia and Yingxin Liu are thanked for their help during the beamline experiments. Veit-Lorentz Heuthe is thanked for helping out with titrations and fruitful discussions regarding orientation parameters. Dr Andrew Kentaro Inge is thanked for performing XRD measurements and related data interpretation.

References

1 R. J. Hamers, *Acc. Chem. Res.*, 2017, **50**, 633–637.
2 A. Livingston, B. L. Trout, I. T. Horvath, M. D. Johnson, L. Vaccaro, J. Coronas, C. W. Babbitt, X. Zhang, T. Pradeep, E. Drioli, J. D. Hayler, K. C. Tam, C. O. Kappe, A. G. Fane and G. Szekely, in *Sustainable Nanoscale Engineering*, ed. G. Szekely and A. Livingston, Elsevier, 2020, pp. 1–18.
3 M.-C. Li, Q. Wu, R. J. Moon, M. A. Hubbe and M. J. Bortner, *Adv. Mater.*, 2021, **33**, 2006052.
4 D. Klemm, F. Kramer, S. Moritz, T. Lindström, M. Ankerfors, D. Gray and A. Dorris, *Angew. Chem., Int. Ed.*, 2011, **50**, 5438–5466.
5 R. J. Moon, A. Martini, J. Nairn, J. Simonsen and J. Youngblood, *Chem. Soc. Rev.*, 2011, **40**, 3941–3994.
6 M. Rajinipriya, M. Nagalakshmaiah, M. Robert and S. Elkoun, *ACS Sustainable Chem. Eng.*, 2018, **6**, 2807–2828.
7 J. D. P. de Amorim, K. C. de Souza, C. R. Duarte, I. da Silva Duarte, F. de Assis Sales Ribeiro, G. S. Silva, P. M. A. de Farias, A. Stingl, A. F. S. Costa, G. M. Vinhas and L. A. Sarubbo, *Environ. Chem. Lett.*, 2020, **18**, 851–869.
8 W. Y. Hamad, *Cellulose Nanocrystals: Properties, Production and Applications*, John Wiley & Sons, 2017.
9 Y. Liu, C. Schütz, G. Salazar-Alvarez and L. Bergström, *Langmuir*, 2019, **35**, 3600–3606.
10 A. Tripathi, B. L. Tardy, S. Khan, F. Liebner and O. J. Rojas, *J. Mater. Chem. A*, 2019, **7**, 15309–15319.
11 M. Giese, L. K. Blusch, M. K. Khan and M. J. MacLachlan, *Angew. Chem., Int. Ed.*, 2015, **54**, 2888–2910.
12 C. Calvino, N. Macke, R. Kato and S. J. Rowan, *Prog. Polym. Sci.*, 2020, **103**, 101221.
13 S. Belbekhouche, J. Bras, G. Siqueira, C. Chappey, L. Lebrun, B. Khelifi, S. Marais and A. Dufresne, *Carbohydr. Polym.*, 2011, **83**, 1740–1748.
14 A. Mihranyan, A. P. Llagostera, R. Karmhag, M. Strømme and R. Ek, *Int. J. Pharm.*, 2004, **269**, 433–442.
15 L. Alves, E. Ferraz and J. A. F. Gamelas, *Adv. Colloid Interface Sci.*, 2019, **272**, 101994.
16 M. Faustini, L. Nicole, E. Ruiz-Hitzky and C. Sanchez, *Adv. Funct. Mater.*, 2018, **28**, 1704158.
17 C. N. Wu, T. Saito, S. Fujisawa, H. Fukuzumi and A. Isogai, *Biomacromolecules*, 2012, **13**, 1927–1932.

Open Access Article. Published on 13 December 2021. Downloaded on 1/21/2026 4:01:33 AM.
This article is licensed under a Creative Commons Attribution 3.0 Unported Licence.

18 U. M. Garusinghe, S. Varanasi, V. S. Raghuwanshi, G. Garnier and W. Batchelor, *Colloids Surf., A*, 2018, **540**, 233–241.
19 Q. Fu, L. Medina, Y. Li, F. Carosio, A. Hajian and L. A. Berglund, *ACS Appl. Mater. Interfaces*, 2017, **9**, 36154–36163.
20 K. M. O. Håkansson, A. B. Fall, F. Lundell, S. Yu, C. Krywka, S. V. Roth, G. Santoro, M. Kvick, L. Prahl Wittberg, L. Wågberg and L. D. Söderberg, *Nat. Commun.*, 2014, **5**, 4018.
21 S. Iwamoto, A. Isogai and T. Iwata, *Biomacromolecules*, 2011, **12**, 831–836.
22 I. Karadagli, B. Schulz, M. Schestakow, B. Milow, T. Gries and L. Ratke, *J. Supercrit. Fluids*, 2015, **106**, 105–114.
23 O. Nechyporchuk, R. Bordes and T. Köhnke, *ACS Appl. Mater. Interfaces*, 2017, **9**, 39069–39077.
24 V. Kumar, A. Elfving, H. Koivula, D. Bousfield and M. Toivakka, *Ind. Eng. Chem. Res.*, 2016, **55**, 3603–3613.
25 B. Wicklein, A. Kocjan, G. Salazar-Alvarez, F. Carosio, G. Camino, M. Antonietti and L. Bergström, *Nat. Nanotechnol.*, 2015, **10**, 277–283.
26 K. M. O. Håkansson, I. C. Henriksson, C. de la Peña Vázquez, V. Kuzmenko, K. Markstedt, P. Enoksson and P. Gatenholm, *Adv. Mater. Technol.*, 2016, **1**, 1600096.
27 V. C. F. Li, A. Mulyadi, C. K. Dunn, Y. Deng and H. J. Qi, *ACS Sustainable Chem. Eng.*, 2017, **6**, 2011–2022.
28 S. Sultan and A. Mathew, *Nanoscale*, 2018, **10**, 4421–4431.
29 D. Kam, M. Chasnitsky, C. Nowogrodski, I. Braslavsky, T. Abitbol, S. Magdassi and O. Shoseyov, *Colloids Interfaces*, 2019, **3**, 46.
30 H. Grützmacher, J. Wang, A. Chiappone, I. Roppolo, F. Shao, E. Fantino, M. Lorusso, D. Rentsch, K. Dietliker and C. F. Pirri, *Angew. Chem., Int. Ed.*, 2017, 1–5.
31 W. J. Orts, L. Godbout, R. H. Marchessault and J.-F. Revol, *Macromolecules*, 1998, **31**, 5717–5725.
32 T. Ebeling, M. Paillet, R. Borsali, O. Diat, A. Dufresne, J. Y. Cavaillé and H. Chanzy, *Langmuir*, 1999, **15**, 6123–6126.
33 H.-N. Xu, Y.-Y. Tang and X.-K. Ouyang, *Langmuir*, 2017, **33**, 235–242.
34 A. D. Haywood, K. M. Weigandt, P. Saha, M. Noor, M. J. Green and V. A. Davis, *Soft Matter*, 2017, **13**, 8451–8462.
35 F. Pignon, M. Challamel, A. De Geyer, M. Elchamaa, E. F. Semeraro, N. Hengl, B. Jean, J. L. Putaux, E. Gicquel, J. Bras, S. Prevost, M. Sztucki, T. Narayanan and H. Djeridi, *Carbohydr. Polym.*, 2021, **260**, 117751.
36 A. M. Philippe, C. Baravian, M. Imperor-Clerc, J. De Silva, E. Paineau, I. Bihannic, P. Davidson, F. Meneau, P. Levitz and L. J. Michot, *J. Phys.: Condens. Matter*, 2011, **23**, 194112.
37 T. Abitbol, E. Kloser and D. G. Gray, *Cellulose*, 2013, **20**, 785–794.
38 S. Beck, M. Méthot and J. Bouchard, *Cellulose*, 2015, **22**, 101–116.
39 M. S. Reid, M. Villalobos and E. D. Cranston, *Langmuir*, 2017, **33**, 1583–1598.
40 J. B. Hopkins, R. E. Gillilan and S. Skou, *J. Appl. Crystallogr.*, 2017, **50**, 1545–1553.
41 K. Manalastas-Cantos, P. V. Konarev, N. R. Hajizadeh, A. G. Kikhney, M. V. Petoukhov, D. S. Molodenskiy, A. Panjkovich, H. D. T. Mertens, A. Gruzinov, C. Borges, C. M. Jeffries, D. I. Svergun and D. Franke, *J. Appl. Crystallogr.*, 2021, **54**, 343–355.
42 M. Park, D. Lee, S. Shin and J. Hyun, *Colloids Surf., B*, 2015, **130**, 222–228.
43 M. Nordenström, A. B. Fall, G. Nyström and L. Wågberg, *Langmuir*, 2017, **33**, 9772–9780.
44 Y. Xu, A. Atrens and J. R. Stokes, *Adv. Colloid Interface Sci.*, 2020, **275**, 102076.
45 A. P. Philipse and A. M. Wierenga, *Langmuir*, 1998, **14**, 49–54.
46 R. A. Schoonheydt and C. T. Johnston, in *Developments in Clay Science*, ed. B. Faïza and G. Lagaly, Elsevier, 2013, vol. 5, pp. 139–172.
47 C. Burger, B. S. Hsiao and B. Chu, *Polym. Rev.*, 2010, **50**, 91–111.
48 P. Li, M. Yang, Y. Liu, H. Qin, J. Liu, Z. Xu, Y. Liu, F. Meng, J. Lin, F. Wang and C. Gao, *Nat. Commun.*, 2020, **11**, 2645.
49 C. Brouzet, N. Mittal, L. D. Söderberg and F. Lundell, *ACS Macro Lett.*, 2018, **7**, 1022–1027.
50 T. Rosén, N. Mittal, S. V. Roth, P. Zhang, F. Lundell and L. D. Söderberg, *Soft Matter*, 2020, **16**, 5439–5449.
51 C. Rosenblatt, R. B. Frankel and R. P. Blakemore, *Biophys. J.*, 1985, **47**, 323–325.
52 J. Van Rie, C. Schütz, A. Gençer, S. Lombardo, U. Gasser, S. Kumar, G. Salazar-Alvarez, K. Kang and W. Thielemans, *Langmuir*, 2019, **35**, 2289–2302.
53 C. Lang, J. Kohlbrecher, L. Porcar, A. Radulescu, K. Sellinghoff, J. K. G. Dhont and M. P. Lettinga, *Macromolecules*, 2019, **52**, 9604–9612.
54 S. J. Bryant, V. Calabrese, M. A. da Silva, K. M. Z. Hossain, J. L. Scott and K. J. Edler, *PLoS One*, 2021, **16**, e0252660.
55 M. Z.-C. Hu, J. T. Zielke, J.-S. Lin and C. H. Byers, *J. Mater. Res.*, 1999, **14**, 103–113.
56 H. D. T. Mertens and D. I. Svergun, *J. Struct. Biol.*, 2010, **172**, 128–141.

 This journal is © The Royal Society of Chemistry 2022